95-GHz Scattering by Terrain at Near-Grazing Incidence

Fawwaz T. Ulaby, *Fellow, IEEE*, Adib Nashashibi, *Member, IEEE*, Alaa El-Rouby, Eric S. Li, Roger D. De Roo, *Member, IEEE*, Kamal Sarabandi, *Senior Member, IEEE*, Ronald J. Wellman, and H. Bruce Wallace

***Abstract*— This study, consisting of three complimentary topics, examines of the millimeter-wave backscattering behavior of terrain at incidence angles extending between 70 and 90°, corresponding to grazing angles of 20° to 0°. The first topic addresses the character of the statistical variability of the radar backscattering cross section per unit area σ_A. Based on an evaluation of an extensive data set acquired at 95 GHz, it was determined that the Rayleigh fading model (which predicts that σ_A is exponentially distributed) provides an excellent fit to the measured data for various types of terrain covers, including bare surfaces, grasses, trees, dry snow, and wet snow. The second topic relates to the angular variability and dynamic range of the backscattering coefficient σ^0, particularly near grazing incidence. In this paper, we provide a summary of data reported to date for each of several types of terrain covers. The last topic focuses on bare surfaces. A semi-empirical model for σ^0 is presented for vertical (VV), horizontal (HH), and cross (HV) polarizations. The model parameters include the incidence angle θ, the surface relative dielectric constant ϵ, and the surface roughness ks, where $k = 2\pi/\lambda$ and s is the surface root mean square (rms) height.**

***Index Terms*—Electromagnetic scattering, rough surfaces.**

I. Introduction

WHEN we characterize the radar backscatter behavior of a target, be that a point target such as a truck, a fence, or an urban feature, or a distributed target such as a field of corn or a forest canopy, we usually do so in terms of two sets of parameters—the target parameters and the sensor parameters. The target parameters include shape factors and dielectric properties and the sensor parameters include the wave frequency f, the incidence angle θ, the receive-transmit polarization configuration [such as horizontally polarized receiver and a vertically polarized transmitter (HV)] and (possibly) the dimensions of the cell illuminated by the radar antenna. In the microwave region, numerous investigations and extensive measurements of the backscatter from terrain have been made over the past three decades at centimeter wavelengths, but much fewer observations have been made at millimeter wavelengths, particularly at high-incidence angles (low-grazing angles). This paper deals with low-grazing-angle terrain backscatter at millimeter wavelengths, with a particular emphasis on 95 GHz.

Manuscript received May 20, 1997; revised October 13, 1997.

F. T. Ulaby, A. Nashashibi, A. El-Rouby, E. S. Li, R. D. De Roo, and K. Sarabandi are with the Radiation Laboratory, EECS Department, University of Michigan, Ann Arbor, MI 48109 USA.

R. J. Wellman and H. B. Wallace are with the Army Research Laboratory, Adelphi, MD 20783 USA.

Publisher Item Identifier S 0018-926X(98)01030-8.

A. Nomenclature

By way of introducing some of the terms we intend to use in this paper, let us consider the hypothetical scene depicted in Fig. 1. The scene consists of several fields of vegetation (grass, for example) at various stages of growth. Each field is *statistically homogeneous*, meaning that it exhibits the same local statistics (in terms of plant height, density, water content, etc.) for any location within that field. The scene is imaged by a distant radar with resolution cell area A at the range corresponding to the scene under consideration. The dimensions of A are such that on the one hand, each cell contains many randomly distributed scatterers, thereby satisfying one of the assumptions of Rayleigh fading statistics [1], while on the other hand, A is much smaller than the overall field dimensions. Because of this latter feature, the number of cells N contained in each field is sufficiently large as to allow us to examine the statistical properties of the radar backscatter variation across a given field. Each cell in the scene is denoted by a combination of two indexes i and j, defined as follows:

i field index with $i = 1, 2, \cdots, M$ fields;

j cell index within a field with $j = 1, 2, \cdots, N$ cells.

The radar response is characterized by the following quantities:

$\sigma_A(i, j) = \sigma(i, j)/A$ radar cross section per unit area of cell (i, j);

$\sigma_i^0 = {}_j\langle\sigma_A(i, j)\rangle = \frac{1}{N}\sum_{j=1}^{N}\sigma_A(i, j)$ scattering coefficient of field i;

$p_i(\sigma_A)$ = probability density function (pdf) of σ_A for all cells of field i;

$p(\sigma_A)$ = probability density function (pdf) of σ_A for all cells of all fields within the scene.

In terms of the scene depicted in Fig. 1, $p_i(\sigma_A)$ might be the pdf of one of the fields of vegetation, whereas $p(\sigma_A)$ would be the pdf for the entire class of vegetation (all fields) present in the scene. We make this distinction for an important reason. Many papers appear in the literature in which the authors have fitted radar backscatter data from heterogeneous terrain, often referred to as radar clutter, to the K distribution [2]–[4]. This does not imply that the Rayleigh fading model [1] is inapplicable. The Rayleigh model is based on three important

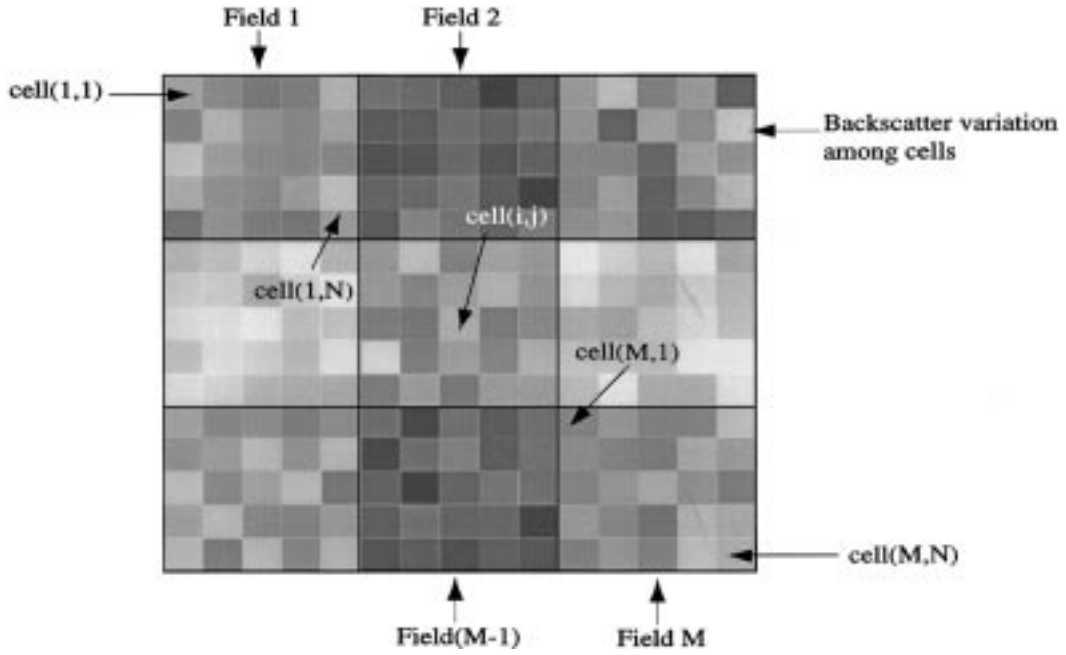

Fig. 1. Depiction of a radar image of a scene consisting of M fields of vegetation with each field occupied by N illuminated cells.

assumptions: 1) each cell should contain several scatterers; 2) the scatterers should be randomly distributed in location so as to satisfy the assumption that the returns are characterized by a uniform phase distribution; and 3) the strengths of the returns from the scatterers are comparable in magnitude or, equivalently, that no individual (or few) scatterer(s) should dominate over the others. These conditions are usually satisfied for any terrain target with statistically homogenous properties, as long as the cell dimensions are much larger than the dimensions of individual scatterers. According to the Rayleigh model, the amplitude of the voltage of the scattered signal is Rayleigh distributed and the amplitude of the power of the scattered signal is exponentially distributed. As we will see later in this paper, $p_i(\sigma_A)$ does indeed fit the exponential distribution (within measurement accuracy) for statistically homogeneous targets (bare soil, gravel, trees, grasses, etc.), but if we were to combine the data from multiple types of terrain targets together into a single data set, the pdf of the combined data will not necessarily be exponentially distributed. In that case, the use of the K distribution to fit $p(\sigma_A)$ of a heterogeneous scene may be quite appropriate.

B. Questions

This paper will attempt to answer the following questions.

1) Is the pdf $p_i(\sigma_A)$ exponentially distributed for seemingly (statistically) homogeneous terrain surfaces when observed at 95 GHz along directions close to grazing incidence?
2) What are the general trends exhibited by σ^0 as a function of angle (in general, but particularly near grazing incidence) at 95 GHz for various types of terrain covers?

In addition to answering these two questions, the paper will also include a semi-empirical model for σ^0 for bare-soil surfaces.

II. Data Sources

The majority of the data presented in this paper was acquired by two instrumentation grade 95-GHz polarimetric scatterometer systems, one belonging to the University of Michigan and the other belonging to the Army Research Laboratory. A brief description of each follows.

A. U–M 95-GHz Polarimetric Scatterometer

The U–M system is a truck-mounted network analyzer-based polarimetric radar system that operates over a bandwidth of up to 2 GHz centered at 95 GHz. Using a coherent-on-receive measurement technique, the system is capable of measuring the Mueller matrix of a target by transmitting (sequentially) six different polarizations [vertical (V), horizontal (H), 45° linear, 135° linear, left-hand circular (LHC), and right-hand circular (RHC)] and receiving simultaneously the V- and H-polarized components of the backscattered field for each transmitted polarization [5]–[7]. The transmitted power level is 3 dBm and calibration is accomplished by employing a calibration technique that uses a metallic sphere and any depolarizing target (whose scattering matrix need not be known) [8]. The procedure provides measurements with an accuracy of ± 1 dB in magnitude, $\pm 5°$ in phase and a cross-pol isolation of 40 dB. The radar uses a 3-in-diameter lens-corrected horn antenna for transmission and a 6-in-diameter lens-corrected horn antenna for reception arranged in a pseudomonostatic mode. The combination produces a two-way beamwidth of 1.4°. For measurements at incidence angles up to 70° from nadir, the system is mounted atop a truck-mounted boom and, for measurements at angles near grazing, the radar is mounted on a computer-controlled gimbal housed inside of a van. The gimbal is used to control the radar look direction in both azimuth and elevation. From a 1.2-m height

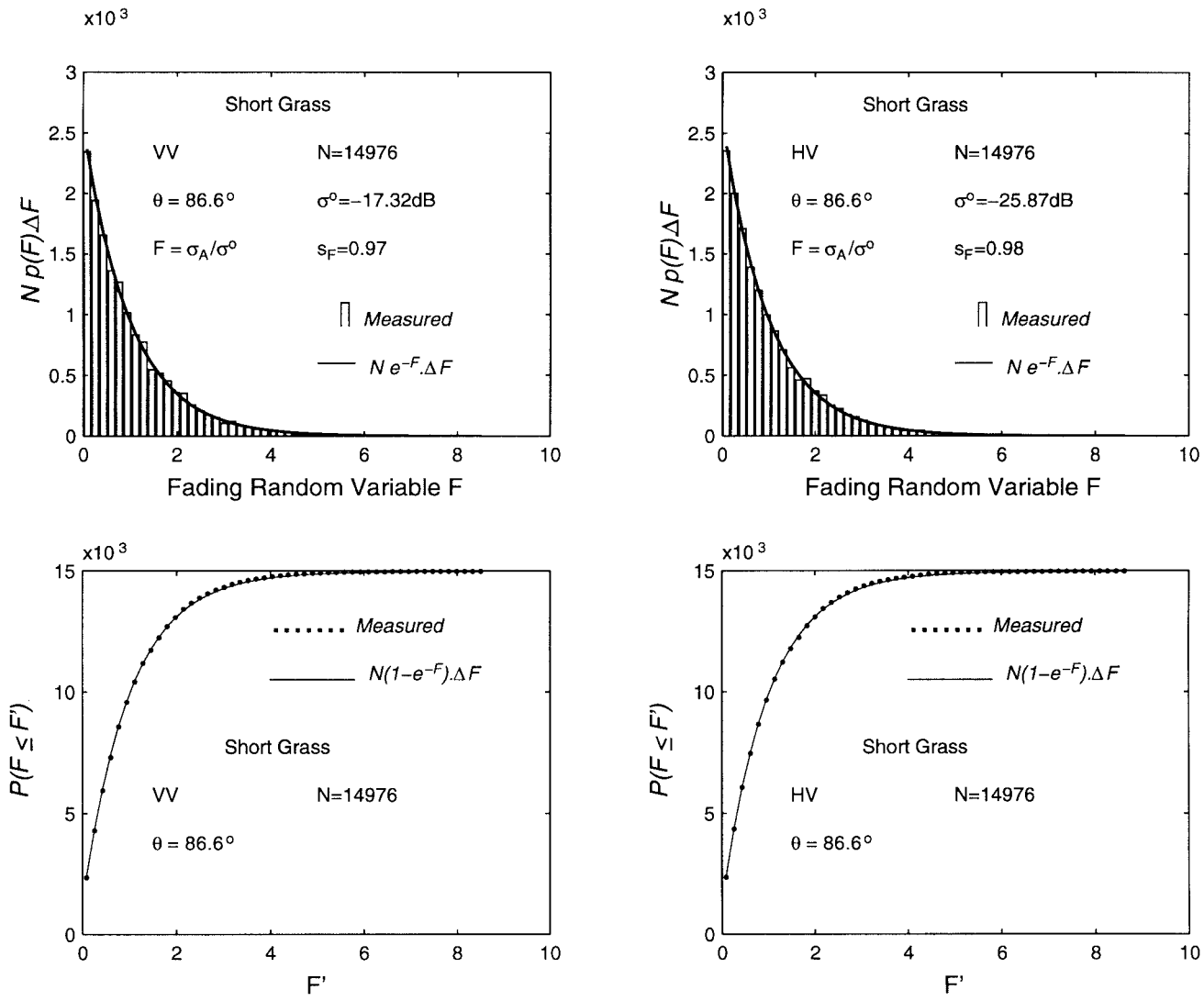

Fig. 2. Comparison of 95-GHz measured histograms of the pdf $p(F)$ and the cumulative distribution $P(F \leq F')$ for grass-covered terrain with theoretical expectations based on the exponential pdf.

above ground level, the illuminated area at a grazing angle of 4°, for example, is 0.42 m in azimuth and 6.2 m in range.

B. ARL 95-GHz Polarimetric Scatterometer

The ARL system is a pulse radar that operates in a frequency stepped mode between 95 and 95.64 GHz [9]. It is configured to transmit 100-ns-long pulses (with an equivalent range resolution of 15 m) at 45-W peak power and a pulse repetition frequency of 10 kHz. Using a 6-in-diameter lens-corrected horn antenna operated in a monostatic mode, the effective two-way antenna beamwidth is 1°. The radar operates in a fully coherent mode and can measure the scattering matrix of a target in either the V/H polarization coordinate system or the LHC/RHC polarization system. A total of five different calibration targets are employed in the calibration procedure. Measurement accuracy is ±1 dB in magnitude, ±5° in phase, and the cross-pol isolation is 35 dB. When deployed in the field for measuring the backscatter of terrain, the radar is mounted on an elevation-over-azimuth computer-controlled pedestal at a height of about 10 m above ground level. At a grazing angle of 3.4°, the dimensions of the ground cell measured by the radar are 2.9 m in azimuth and about 15 m in range.

In addition to reporting data acquired by the two radar systems described above, we will also include some 95-GHz data acquired by the University of Massachusetts polarimetric scatterometer system [10]–[12]. Some of that data is available in a joint U–M/U–Mass millimeter-wave radar data handbook [13].

III. Radar Backscatter Statistics

For a statistically homogeneous target, such as field i in Fig. 1, the Rayleigh model states that the backscattering cross section per unit area, $\sigma_A(i, j)$, behaves like a random variable with an exponential pdf given by

$$p_i(\sigma_A) = \begin{cases} \dfrac{1}{\sigma_i^0} \exp(-\sigma_A/\sigma_i^0), & \text{for } \sigma_A \geq 0 \\ 0, & \text{for } \sigma_A < 0 \end{cases} \tag{1}$$

where σ_i^0 is the backscattering coefficient of field i. It is called a Rayleigh fading model because the electric field of the received signal, which is proportional to $\sqrt{\sigma_A}$, is Rayleigh distributed. By introducing the fading random variable $F = \sigma_A/\sigma_i^0$, we can express σ_A as a product of the form

$$\sigma_A = \sigma_i^0 F \tag{2}$$

with

$$p(F) = \begin{cases} e^{-F}, & \text{for } F \geq 0 \\ 0, & \text{for } F < 0. \end{cases} \tag{3}$$

For the exponential pdf given by (3), the mean value $\overline{F}$ and standard deviation s_F of the normalized random variable F are

$$\overline{F} = s_F = 1. \tag{4}$$

The validity of the exponential pdf was examined using data recorded by the two 95-GHz systems described in the preceding section for each of the following types of terrain: 1) bare surfaces, including soil, gravel, concrete, and asphalt; 2) grasses, including both dense short grasses and sparse tall grasses; 3) deciduous trees; 4) coniferous trees; 5) dry snow cover; and 6) wet snow cover. The examination was performed over several incidence angles ranging between 70 and 88° for each of the three principal linear polarizations—VV, HV, and HH. In each individual examination, we generated histograms of the pdf $p(F)$ and of the cumulative distribution

$$P(F \leq F') = \int_0^{F'} p(F)\, df. \tag{5}$$

An example of the results is shown in Fig. 2 for grasses where a total of 14 976 data points were available at $\theta = 86.6°$. The scene observed by the radar contained many cells that were grass covered. Each of these were observed at 64 equally spaced (10 MHz) different frequencies extending between 95 and 95.64 GHz. For a system with a range resolution $\Delta R = 15$ m, the decorrelation bandwidth Δf is given by [1, p. 72]

$$\Delta f \simeq \frac{150}{\Delta R} \text{ MHz } = 10 \text{ MHz}. \tag{6}$$

Hence, the multifrequency radar observations are statistically independent, which means that the total number of statistically independent samples of σ_A of grass available from a given mission (one-time observation of a scene) is $64N_c$, where N_c is the number of terrain cells covered with grass. The radars were used to make observations at different times during the day, as well as on different days. Each of these observations is called a mission. The average value of σ_A, namely σ_i^0 for field i, may change between missions due to physical changes in the grass cover or underlying soil surface. Hence, before combining data from different missions we normalized the data associated with a given mission to the mean value for that mission. Through this process we were able to generate data sets with large values of N, while avoiding the problem of mixing up targets of different types or targets under different conditions. The process is equivalent to normalizing σ_A of the cells of each of the fields in Fig. 1 to the mean value for that field before combining the data from all the cells for all the fields. The total number of independent samples is then

$$N = 64N_cN_m \tag{7}$$

where N_c is the number of cells in a mission and N_m is the number of missions. In the case of the grass-covered terrain whose $p(F)$ and $P(F \leq F')$ are shown in Fig. 2, $N = 14\,976$. We note that the calculated value of the standard deviation s_F is 0.97 for VV polarization and 0.98 for HV polarization, both of which are very close to the theoretical value of 1.0 given by (4). Also, the measured data exhibits excellent agreement with the exponential model.

The example depicted in Fig. 2 for grass-covered terrain is typical of all the combinations of terrain covers, incidence angles, and polarizations examined in this study. The terrain cover that exhibited the greatest deviation from the typical behavior for grass is trees and even then the agreement with the exponential pdf predicted by the Rayleigh fading model is very good, as demonstrated by the data presented in Fig. 3 for deciduous trees. It is important to note that the data for trees does not include mixed categories; a cell observed by the radar is defined to belong to the terrain category called trees only if the cell contains trees and no other categories. Thus, a cell that was partially a ground surface and partially a tree was excluded from consideration.

IV. Angular Response of σ^0

With the exception of electromagnetically smooth surfaces, our data base of 95-GHz measurements of the radar backscatter from terrain shows that the VV-polarized and HH-polarized levels of the backscattering coefficients are always within 2 dB of one another regardless of incidence angle and in most cases the difference in level is close to zero. The backscatter response of bare soil surfaces will be the subject of the next section of this paper, where we will examine the behavior of the copolarized ratio $\sigma_{hh}^0/\sigma_{vv}^0$ explicitly. Hence, we have decided to limit our discussion in the present section to the VV-polarized and HV-polarized components only. The data displayed in Figs. 4–8 covers the incidence-angle range from 60 to 90°. The terrain classes include bare surfaces (including bare soil, asphalt, and gravel), grasses, trees, dry snow cover, and wet snow cover. For each terrain class, the displayed data comes from multiple sources and each source consists of multiple observations, often made at different locations and for different terrain conditions. That is why the data for grass (Fig. 5), for example, exhibits a significant change in level between 70 and 74°; the data at 60 and 70° belong to a measurement set different from that of the data at the higher angles.

Examination of the data presented in Figs. 4–8 leads to the following observations.

1) The backscatter from terrain observed by a radar is a result of surface scattering, volume scattering, or some combination of both scattering mechanisms. For the

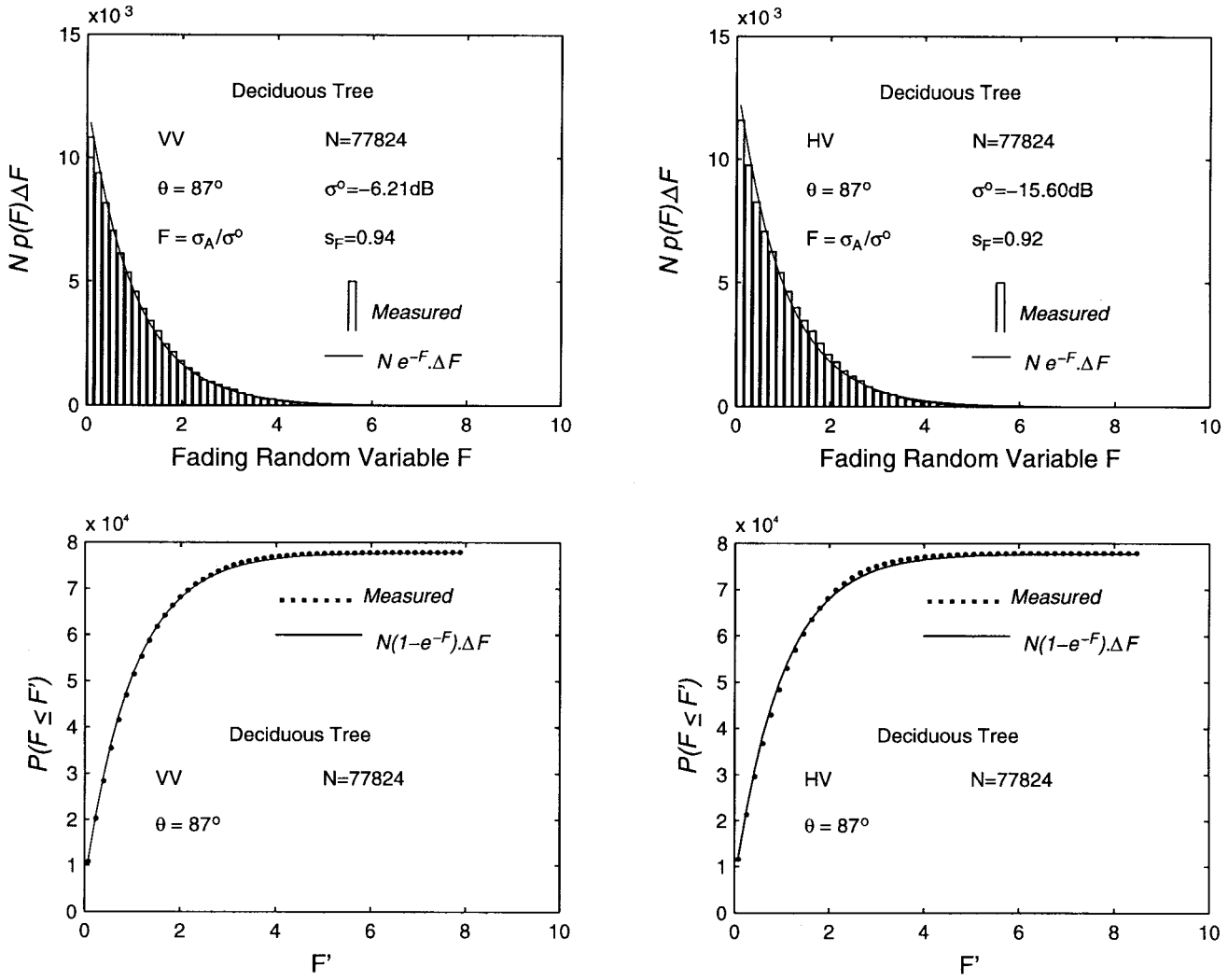

Fig. 3. Comparison of 95-GHz measured histograms of the pdf $p(F)$ and the cumulative distribution $P(F \leq F')$ for tree-covered terrain with theoretical expectations based on the exponential pdf.

surfaces represented by Fig. 4, σ^0 exhibits a negative slope with incidence angle, with steeper slopes associated with the smoother surfaces (the highest level values correspond to very rough surfaces and lowest level values correspond to a very smooth surface). The data in Figs. 5–8, corresponding to grasses, trees, and dry and wet snow, indicate that the angular variation of σ^0 is comparable to that of rough surfaces.

2) At any given angle and for any particular polarization, the dynamic range for a given terrain class can be as large as 20 dB or more. In the case of surfaces, the variation is in response to roughness and moisture content. The vegetation classes (grasses and trees) exhibit σ^0 variations due to density, height, shape, and moisture content, and the backscatter by snow is governed by crystal size, liquid water content, snow depth, and snow density [14]–[16].
3) Fig. 9 displays the upper and lower boundaries of the envelope containing all σ° values for all terrain categories combined. The dynamic range for each of the polarizations increases from about 15 dB for VV polarization and 20 dB for HV polarization at 60° to close to 40 dB for both polarizations at 88°. The dynamic range for HH polarization (not shown) is comparable to that for VV polarization.

V. Backscattering Model for Rough Surfaces

A random surface is one whose two-dimensional height profile $z(x, y)$ varies randomly (nondeterministically) as a function of spatial position. The vertical variation of such a surface is characterizable in terms of the height probability density function $p(z)$. For most natural surfaces, $p(z)$ is a zero-mean Gaussian function [17] with a rms height (standard derivation) s. The range that s exhibits may extend between about 0.5 mm for an artificially prepared surface that has been smoothed out by a highway construction roller, up to about 4 cm for a freshly plowed field.

The horizontal variation of the height $z(x, y)$ may be described by the correlation function $\rho[z_1(x_1, y_1); z_2(x_2, y_2)]$ where z_1 and z_2 are the heights at locations (x_1, y_1) and (x_2, y_2). Most natural surfaces tend to be azimuthally sym-

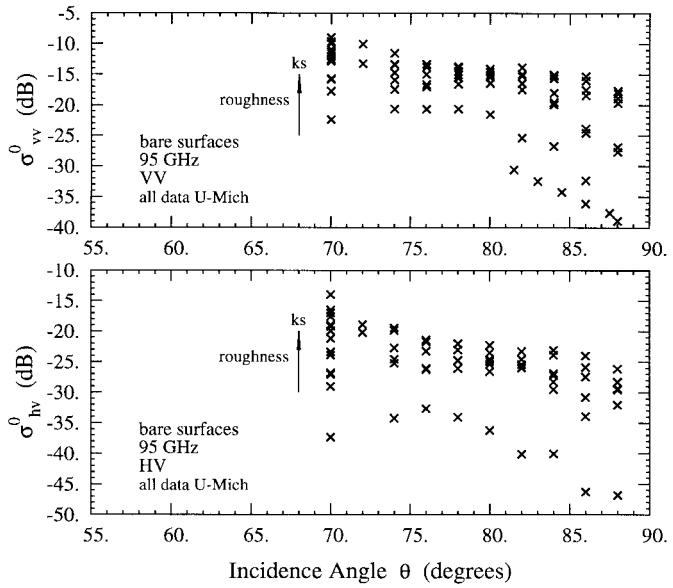

Fig. 4. Measured values of σ^0 at 95 GHz for VV and HV polarizations for bare surfaces, including gravel, asphalt, concrete, and bare agricultural fields.

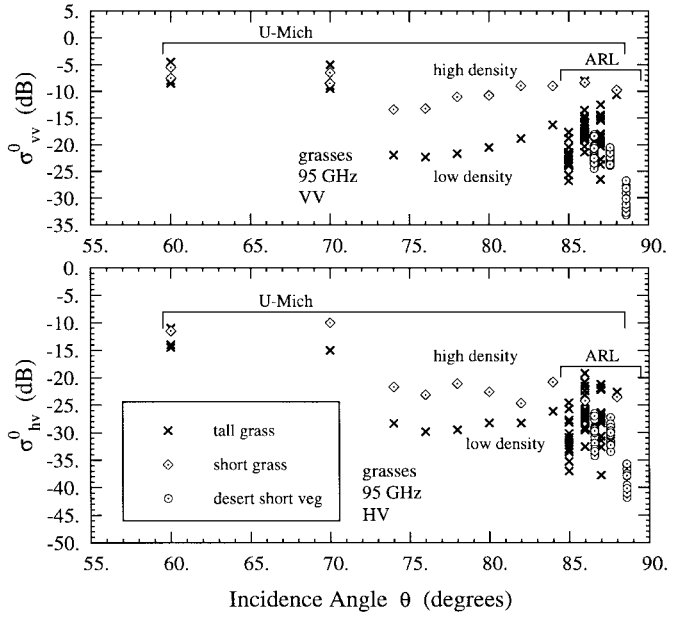

Fig. 5. Measured values of σ^0 at 95 GHz for VV and HV polarizations for grass-covered terrain.

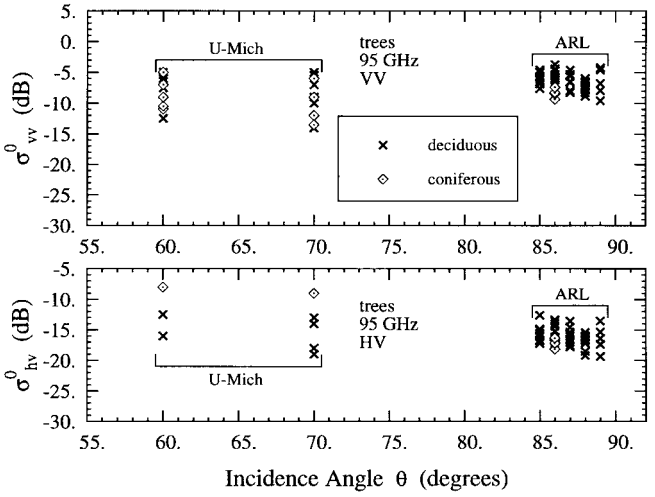

Fig. 6. Measured values of σ^0 at 95 GHz for VV and HV polarizations for tree-covered terrain, including both deciduous and coniferous trees.

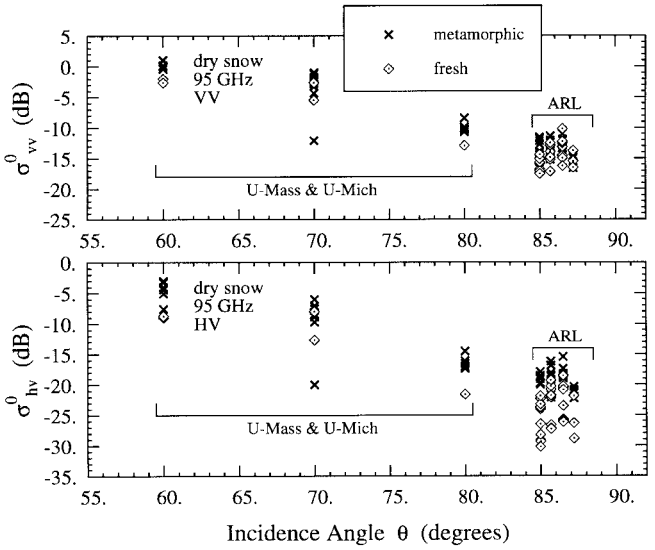

Fig. 7. Measured values of σ^0 at 95 GHz for VV and HV polarization for dry snow-covered terrain.

metric as well as statistically stationary, which means that ρ does not depend on the specific locations of the two points, but instead depends on the distance r between them in which case we write the surface correlation function simply as $\rho(r)$. Whereas measuring the height distribution $p(z)$ and determining the rms height s are manageable tasks in practice (it is fairly difficult to measure s with an accuracy better than ± 0.5 mm), the same is not true with regard to $\rho(r)$. To measure $\rho(r)$ with an accuracy compatible with analytical or numerical calculations of radar backscattering from a surface, it is necessary to sample the surface height 1) in two dimensions; 2) at a spacing no greater than $\lambda/10$ where λ is the radar wavelength; and 3) over a surface segment no shorter than 10ℓ, where ℓ is the surface correlation length. For a typical soil surface with $\ell = 10$ cm observed at an X-band wavelength $\lambda = 3$ cm, the sampling requirement translates into measuring a 1 m $\times$ 1 m segment at a spacing of 3 mm in both the x- and y-directions. These requirements represent the capability limits of a high-resolution laser ranging system, which is not only difficult to set up and operate outside of a laboratory environment, but it would also take it several hours of measurement time to sample the surface at the required spacing. At shorter wavelengths, the sampling requirement is even more stringent and consequently impossible to meet in practice.

In general, all random-surface scattering models are intimately coupled to two physical parameters: 1) the complex dielectric constant of the surface, ϵ and 2) the surface roughness parameters s and $\rho(r)$ [18]. Because of the difficulty associated with measuring $\rho(r)$ for outdoor surfaces under natural conditions, it has been somewhat difficult to evaluate

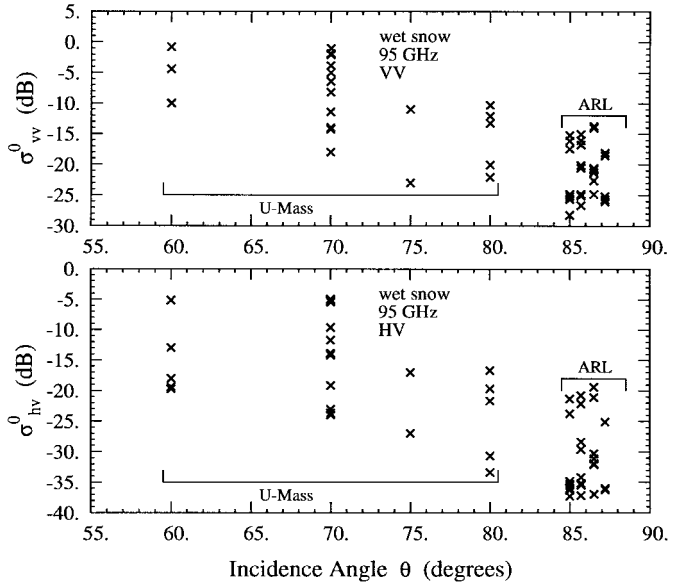

Fig. 8. Measured values of σ^0 at 95 GHz for VV and HV polarization for wet snow-covered terrain.

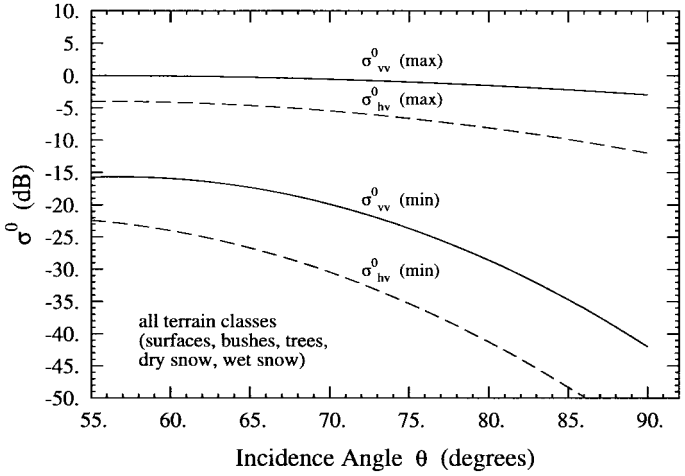

Fig. 9. Dynamic range of σ^0 for terrain at 95 GHz. The maximum and minimum curves represent the upper and lower bounds between which all measured values are contained.

the applicability of theoretical models and to compare their predictions with experimental observations. This has led to greater reliance on the development of semi-empirical models for characterizing radar scattering by terrain, where semi-empirical refers to mathematical expressions that match the behavior of the experimental data, but are also cast in a form that adheres to the general behavior of theoretical models. For example, scattering theory predicts that a surface will exhibit VV and HH backscattering coefficients of equal magnitude when the scale of roughness (represented by the rms height s) becomes very large compared to λ. Hence, a good semi-empirical model should reflect such a trend.

Based on field investigations conducted over the past eight years, we have developed such semi-empirical models for two ranges of the microwave spectrum. The first study covered the 1–10 GHz range in frequency and the 20–70° range in incidence angle [17]. The second study dealt with the same angular range, but the observations were made at 35 and 95 GHz [7]. More recently, we have undertaken an investigation to examine the backscattering behavior of a variety of different rough surfaces, all at 95 GHz, but over the incidence angle range from 70 to 88° or, equivalently, over the grazing-angle range from 2 to 20°. This section provides an overview of the observed radar backscatter at 95 GHz at low-grazing angles and presents a semi-empirical model that was generated by extending the angular range of the previously published model.

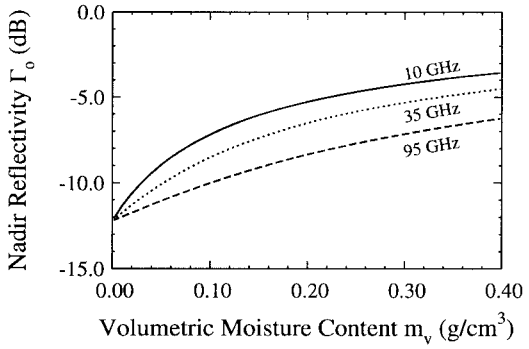

Fig. 10. Nadir reflectivity Γ_0 plotted as a function of soil moisture content at 10, 35, and 95 GHz.

A. Sensitivity to Roughness and Moisture Content

We do know that at a given frequency, the moisture content of a soil medium determines the soil's dielectric constant and that the dielectric constant, in turn, determines the Fresnel reflectivities of the surface, but we do not know the exact form of the relationship between the backscattering coefficient σ° of a real random surface and its H- and V-polarized reflectivities. According to the geometric optics model [18], $\sigma^\circ(\theta)$ of a very rough surface is directly proportional to Γ_0, the nadir reflectivity of the surface, regardless of the incidence angle θ. Since at millimeter wavelengths most natural surfaces are quite rough electromagnetically, we can use Γ_0 to examine the expected sensitivity of σ° to soil moisture content. Fig. 10 shows curves of Γ_0 versus volumetric moisture content, calculated using the soil dielectric model given in Appendix E of Ulaby *et al.* [19]. Even though the model was developed on the basis of microwave data, it is assumed to be valid at millimeter-wave frequencies as well. With the exception of very dry desert-like environments, the moisture content of naturally occurring soils is rarely below 0.05 g/cm^3 and it usually cannot support moisture contents greater than 0.4 g/cm^3. Over this range, the dynamic range is about 5.5 dB at 10 GHz, but less than 3 dB at 95 GHz. Hence, most of the variation exhibited by σ° at 95 GHz would be due to surface roughness.

To illustrate the importance of surface roughness, we show in Fig. 11 plots of σ° versus incidence angle for two surfaces, a relatively smooth surface with $ks = 1.6$ (where $k = 2\pi/\lambda$) and a rough surface with $ks = 8.7$. The difference in level increases with increasing incidence angle for both σ°_{vv} and σ°_{hv} (σ°_{hh} exhibits a similar behavior also). The solid curves shown in the figures were generated on the basis of the model discussed in the next subsection.

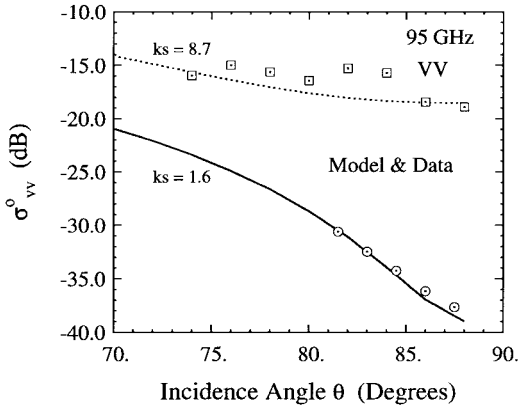

(a)

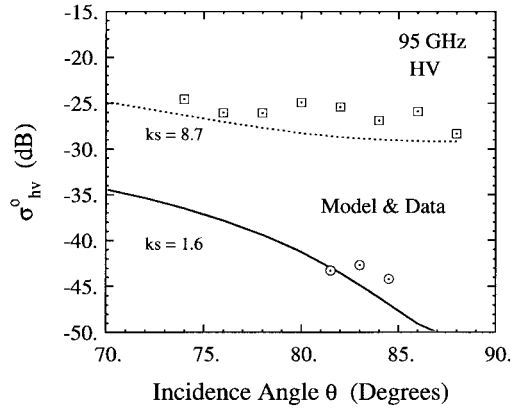

(b)

Fig. 11. VV and HV backscatter responses of a relatively smooth soil surface with $ks = 1.6$ and a rough surface with $ks = 8.7$ at 95 GHz. The continuous curves were calculated on the basis of the model given in the text.

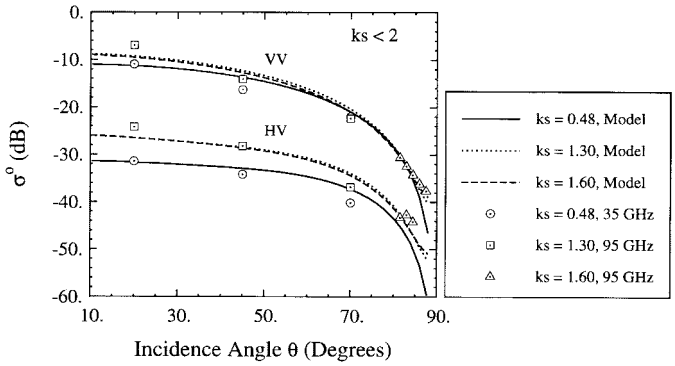

Fig. 12. Measured values of the VV and HV backscattering coefficients, plotted as a function of incidence angle for three different surface roughnesses, all characterized by $ks < 2$. The continuous curves are based on the model given in the text.

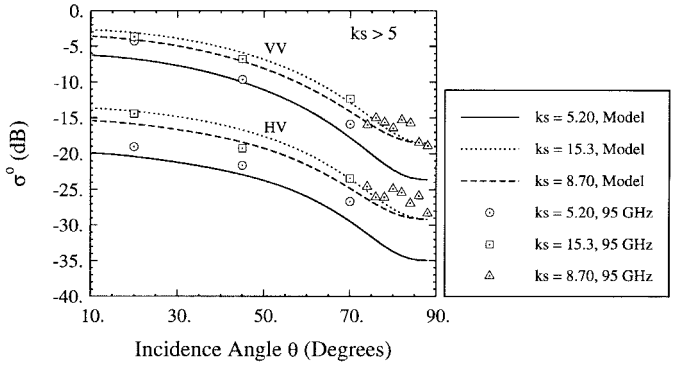

Fig. 13. Measured values of the VV and HV backscattering coefficients, plotted as a function of incidence angle for three different surface roughnesses, all characterized by $ks > 5$. The continuous curves are based on the model given in the text.

B. Two-Component Roughness Model

All theoretical surface scattering models predict that σ° should decrease very rapidly in magnitude as θ approaches grazing incidence. Analysis of the experimental measurements that we conducted at 35 and 95 GHz, over a range of surface roughness extending between $ks = 0.48$ and 15.3, suggests that a surface exhibits one of two types of scattering patterns depending on its ks value. For surfaces with $ks < 2$, σ^0 continues to decrease with increasing θ at a fairly steep slope up to 88°, the maximum angle for which we have measurements. This behavior is illustrated in Fig. 12 for VV and HV polarizations. In contrast, when $ks > 5$ (Fig. 13), σ° exhibits a rather gentle slope with angle. These two types of angular scattering patterns near grazing incidence suggest that perhaps the scattering is the sum of two mechanisms, one due to predominantly horizontal surface facets and another due to predominantly vertical surface facets, similar to the sketch shown in Fig. 14. The horizontal facets would exhibit an angular dependence for σ° that varies as $\cos^2\theta$, whereas the vertical facets would exhibit a $\sin^2\theta$ dependence (similar to a dipole). Both scattering mechanisms are proportional to the nadir reflectivity Γ_0 and each is a function of surface roughness (ks). Functional forms for σ^0_{vv}, σ^0_{hh}, and σ^0_{hv} were generated empirically. The results are

$$\sigma^0_{vv} = \frac{\Gamma_0}{\sqrt{p}}(4.4[1-\exp(-0.15ks\,\cos\theta)]\,\cos^2\theta + 0.1 \quad (8)$$

$$\{1-\exp[-0.000\,67(ks)^4]\}\sin^2\theta) \quad (9)$$

$$\sigma^0_{hh} = p\sigma^0_{vv} \quad (10)$$

$$\sigma^0_{hv} = q\sigma^0_{vv} \quad (11)$$

where

$$p = [1-(2\,\theta/\pi)^{1/(3\Gamma_0)}\,e^{-0.4ks}]^2 \quad (12)$$

$$q = 0.23\,\Gamma_0^{1/2}\,\{1-\exp[-ks(0.27\,\theta^3 - 0.14\,\theta^2 + 0.016\,\theta + 0.17)]\} \quad (13)$$

$$\Gamma_0 = \left|\frac{\sqrt{\epsilon}-1}{\sqrt{\epsilon}+1}\right|^2 \quad (14)$$

with $\epsilon = \epsilon' - j\epsilon''$ being the relative dielectric constant of the soil medium and θ is the incidence angle in radians. The model equations are the basis for all of the calculated curves shown in Figs. 11–13.

We close this section by showing in Fig. 15 plots of the copolarized and cross-polarized ratios p and q, respectively, as a function of ks at two incidence angles. The plots for p were calculated using (12) with $\Gamma_0 = 0.13$, corresponding to a volumetric soil moisture content of 0.18 g/cm^3. The data points shown in the figure had varying values of moisture,

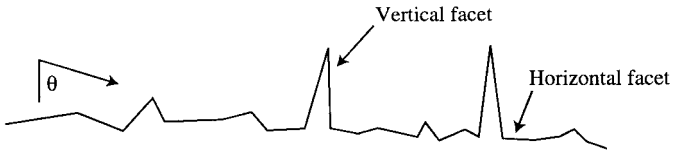

Fig. 14. Sketch of a surface profile depicting a surface that consists of horizontal and vertical facets of various sizes.

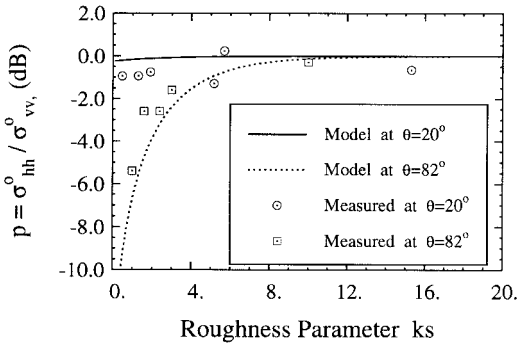

(a)

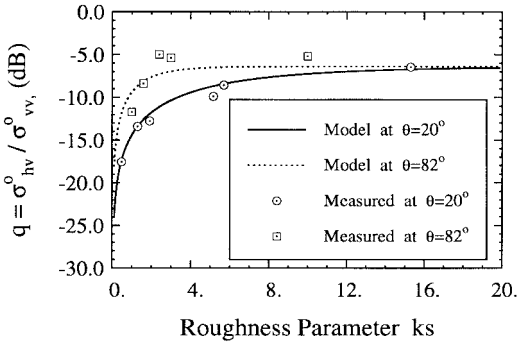

(b)

Fig. 15. Copolarized ratio p and the cross-polarized ratio q, both plotted as a function of surface roughness ks. The continuous curves for p are based on (12) with $\Gamma = 0.13$ and the curves for q are based on (13) with $\Gamma_0 = 1$.

with a low of 0.15 g/cm^3 and a high of 0.24 g/cm^3. In the case of q, the form of (13) allowed us to generate plots for $\Gamma_0 = 1$ and to convert the data points to the same reference. For $ks > 4$, p approaches 1 (0 dB) and q approaches -6.4 dB.

VI. Concluding Remarks

This study reaffirms that the Rayleigh fading model is applicable for characterizing the statistical behavior of radar backscatter for statistically homogeneous, distributed targets such as terrain surfaces as long as the illuminated cell is large enough to contain many scatterers and, additionally, no single (or few) scatterer(s) dominate over all others. In some studies reported in the literature [2], [3], it was stated that the pdf of the backscattering cross section per unit area $p(\sigma_A)$ exhibited a long tail requiring the use of the K distribution to fit the data. Such a behavior was not observed in the present study. A possible explanation for this difference between this and the other studies is that the data in the other studies, which is based on high-resolution synthetic aperture radar (SAR) images of terrain, most likely included heterogeneous terrain consisting of several different terrain types. Furthermore, the data may have included nonterrain targets or some of the pixels may have contained only one or two dominant scatterers, thereby violating one of the tenets of the Rayleigh model. Such a situation can easily arise if the pixel of a high-resolution radar image contains a single trunk of a tree and the trunk-ground combination behaves like a strong corner reflector.

Two other major contributions of this study are the documentation of the dynamic range exhibited by σ^0 for various terrain types, angles, and polarization combinations, and the introduction of a semi-empirical model for characterizing σ^0 of bare surfaces in terms of physical parameters of the surface.

References

[1] F. T. Ulaby and M. C. Dobson, *Handbook of Radar Scattering Statistics for Terrain.* Norwood, MA: Artech, 1989.
[2] J. K. Jao, "Amplitude distribution of composite terrain radar clutter and the K-distribution," *IEEE Trans. Antennas Propagat.*, vol. AP-32, pp. 1049–1062, Oct. 1984.
[3] S. H. Yueh, J. A. Kong, J. K. Jao, R. T. Shin, and L. M. Novak, "K-distribution and polarimetric terrain radar clutter," *J. Electromagn. Waves Applicat.*, vol. 3, no. 8, pp. 747–768, 1989.
[4] E. Jakeman, "On the statistics of K-distributed noise," *J. Phys. A*, vol. 13, pp. 31–48, 1980.
[5] F. T. Ulaby, M. Whitt, and K. Sarabandi, "AVNA-based polarimetric scatterometers," *IEEE Antennas Propagat. Mag.*, vol. 32, pp. 5–17, Oct. 1990.
[6] F. T. Ulaby and C. Elachi, *Radar Polarimetry for Geoscience Applications.* Norwood, MA: Artech, 1990.
[7] A. Nashashibi, F. T. Ulaby, and K. Sarabandi, "Measurement and modeling the millimeter-wave backscatter response of soil surfaces," *IEEE Trans. Geosci. Remote Sensing*, vol. 34, pp. 561–572, Mar. 1996.
[8] A. Nashashibi, K. Sarabandi, and F. T. Ulaby, "A calibration technique for polarimetric coherent-on-receive radar systems," *IEEE Trans. Antennas Propagat.*, vol. 43, pp. 396–404, Apr. 1995.
[9] R. Wellman, G. Goldman, J. Silvious, and D. Hutchins, "Analyses of millimeter wave radar low-angle ground-clutter measurements for European-like and desert environments," Army Res. Lab, Adelphi, MD, Tech. Rep. ARL-TR-1102, July 1996.
[10] P. S. Chang, J. B. Mead, E. J. Knapp, G. A. Sadowy, R. E. Davis, and R. E. McIntosh, "Polarimetric backscatter from fresh and metamorphic snowcover at millimeter wavelengths," *IEEE Trans. Antennas Propagat.*, vol. 44, pp. 58–73. Jan. 1996.
[11] J. B. Mead, P. S. Chang, S. P. Lohmeier, P. M. Langlois, and R. E. McIntosh, "Polarimetric observations and theory of millimeter wave backscatter from snowcover," *IEEE Trans. Antennas Propagat.*, vol. 41, pp. 38–46, Jan. 1993.
[12] J. B. Mead, A. L. Pazmany, P. S. Chang, and R. E. McIntosh, "Comparisons of coherent and noncoherent polarimetric radar measurement techniques at 95 GHz," *Radio Sci.*, vol. 31, no. 2, pp. 325–333, Mar./Apr. 1996.
[13] F. T. Ulaby, R. McIntosh, and W. Flood, Eds., "Handbook of millimeter-wave polarimetric radar response of terrain," Univ. Michigan Radiation Lab. Rep., Ann Arbor, MI, Mar. 1995.
[14] Y. Kuga, F. T. Ulaby, T. F. Haddock, and R. D. DeRoo, "Millimeter-wave radar scattering from snow: I—Radiative transfer model," *Radio Sci.*, vol. 26, no. 2, pp. 329–341, 1991.
[15] F. T. Ulaby, T. F. Haddock, R. T. Austin, and Y. Kuga, "Millimeter-wave radar scattering from snow: II—Comparison of theory with experimental observation," vol. 26, no. 2, pp. 343–351, 1991.
[16] F. T. Ulaby, P. Siqueira, A. Nashashibi, and K. Sarabandi, "Semi-empirical model for radar backscatter from snow at 35 and 95 GHz," *IEEE Trans. Geosci. Remote Sensing*, vol. 34, pp. 1059–1065, Sept. 1996.
[17] Y. Oh, K. Sarabandi, and F. T. Ulaby, "An empirical model and an inversion technique for radar scattering from bare soil surfaces," *IEEE Trans. Geosci. Remote Sensing*, vol. 30, pp. 370–381, Mar. 1992.
[18] F. T. Ulaby, R. K. Moore, and A. K. Fung, *Microwave Remote Sensing.* Norwood, MA: Artech, 1982, vol. II, ch. 12.
[19] ——, *Microwave Remote Sensing.* Norwood, MA: Artech, 1986, vol. III, Appendix E.

Fawwaz T. Ulaby (M'68–SM'74–F'80) received the B.S. degree in physics from the American University of Beirut, Lebanon, in 1964, and the Ph.D. degree in electrical engineering from the University of Texas, Austin, in 1968.

He is the Williams Distinguished Professor of electrical engineering and computer science at the University of Michigan, Ann Arbor, as well as the Director of the Radiation Laboratory there. His current interests include microwave and millimeter-wave remote sensing, radar systems, and radio-wave propagation and he has authored ten books and published over 500 papers and reports on these subjects.

Dr. Ulaby has been the recipient of numerous awards, including the IEEE Geoscience and Remote Sensing Distinguished Achievement Award in 1983, the IEEE Centennial Medal in 1984, the American Society of Photogrammetry's Presidential Citation for Meritorious Service in 1984, the NASA Group Achievement Award in 1990, and the University of Michigan's Distinguished Faculty Achievement Award in 1991. He served as President of the IEEE Geoscience and Remote Sensing Society (1980–1982), Executive Editor of IEEE TRANSACTIONS ON GEOSCIENCE AND REMOTE SENSING (1983–1985), and General Chairman of several international symposia. He is a member of the National Academy of Engineering and serves on several scientific boards and professional committees.

Adib Nashashibi (S'82–M'95) received the B.Sc. and M.Sc. degrees in electrical engineering from Kuwait University, Kuwait, in 1985 and 1988, respectively, and the Ph.D. degree in electrical engineering from the University of Michigan, Ann Arbor, in 1995.

His currently an Assistant Research Scientist at the Radiation Laboratory at the University of Michigan. His research interests include microwave remote sensing, polarimetric millimeter-wave radars, calibration and measurement techniques, electromagnetic-wave propagation, and scattering in random media.

Alaa El-Rouby received the B.Sc. and M.Sc. degrees in electrical engineering from Cairo University, Giza, Egypt, in 1993 and 1996, respectively. He is currently working toward the Ph.D. degree in electrical engineering at the University of Michigan, Ann Arbor.

His current research interests include millimeter-wave polarimetric remote sensing and scattering from natural terrain.

Eric S. Li received the B.S. degree from Tamkang University, Taipei, Taiwan, in 1986, and the M.S. degree in electrical engineering from the State University of New York, Stony Brook, NY, in 1987. He is currently working toward the Ph.D. degree in electrical engineering at the University of Michigan, Ann Arbor.

From 1988 to 1992, he worked as a Microwave Engineer in the cellular phone industry. His current research interests include polarimetric millimeter-wave radar systems, calibration and measurement technique, electromagnetic scattering, and millimeter-wave remote sensing.

Roger D. De Roo (S'88–M'96) received the B.S. degree in letters and engineering from Calvin College, Grand Rapids, MI, in 1986, and the B.S.E., M.S.E., and Ph.D. degrees from the University of Michigan, Ann Arbor, in 1986, 1989, and 1996, respectively, all in electrical engineering.

He is currently employed as a Research Fellow at the University of Michigan. His current research interests include modeling and measurement of bistatic scattering of electromagnetic waves from rough surfaces, inversion of soil moisture and vegetation parameters from the radar signatures of crops, industrial applications of millimeter-wave radiometry, and backscattering phenomenology of natural and man-made objects at near-grazing incidence for millimeter radars.

Kamal Sarabandi (S'87–M'90–SM'92) received the B.S. degree in electrical engineering from Sharif University of Technology, Tehran, Iran, in 1980, and the M.S.E. (electrical engineering), in 1986, and the M.S. (mathematics) and Ph.D. (electrical engineering) degrees in 1989, all from the University of Michigan, Ann Arbor.

From 1980 to 1984, he worked as a Microwave Engineer in the Telecommunication Research Center, Teheran, Iran. He is currently an Associate Professor in the Department of Electrical Engineering and Computer Science at the University of Michigan. He has 15 years of experience with microwave sensors and radar systems. In the past seven years he has served as the Principal Investigator and Co-Investigator on many projects sponsored by NASA, the Jet Propulsion Laboratory, the U.S. Army Research Office, the Office of Naval Research, and General Motors, all related in one way or another to microwave and millimeter-wave radar remote sensing. He has published four book chapters and more than 60 papers in refereed journals on electromagnetic scattering, random media modeling, microwave measurement techniques, radar calibration, application of neural networks in inverse scattering problems, and microwave sensors. He has also had more than 110 papers and presentations in national and international conferences and symposia on similar subjects.

Dr. Sarabandi is listed in *Who's Who in Electromagnetics*. He served as the Chairman of the Geoscience and Remote Sensing Society Southeastern Michigan chapter from 1991 to 1997. He is a member of Commission F of URSI and of the Electromagnetic Academy. He was a recipient of a 1996 Teaching Excellence Award and the 1997 Henry Russel Award from the Regent of the University of Michigan.

Ronald J. Wellman received the B.S. degree in physics and the M.S. degree in electrical engineering from the University of Maryland, College Park, in 1971 and 1979, respectively.

He has been employed by the U.S. Army's Harry Diamond Laboratories (now known as the Army Research Laboratory), Adelphi, MD, since 1971. During the first ten years of his employment, his work was primarily in lasers, laser effects, and optical fusing. Since 1980, he has worked exclusively in the millimeter-wave region of the electromagnetic spectrum. His initial work included the characterization of snow, rain, dust, and smokes at 95, 140, and 225 GHz. More recently, he was the Chief Designer of a fully polarimetric 95-GHz monopulse radar to be used in the measurement of targets and backgrounds for support of smart weapon technology.

H. Bruce Wallace received the B.A. degree in physics from the Johns Hopkins University, Baltimore, MD, in 1971, and the M.S.E.E. degree from the University of Delaware, Newark, in 1984.

In 1971, he entered the U.S. Army as a Lieutenant in the Ordinance Corps. In 1974 he left the army to join the U.S. Army Research Laboratory, Adelphi, MD, where he joined the Concepts Analysis Laboratory investigation of the application of millimeter-wave techniques to weapon systems. His work includes studies in components, atmospheric and near-earth propagation, active and passive system designs, and high-resolution polarimetric imaging. He is currently Chief of the Radio Frequency and Electronics Division, Sensors and Electron Device Directorate of the Army Research Laboratory.